Pergamon

Int. J. Solids Structures Vol. 35, No. 17, pp. 2057–2071, 1998

0020-7683/98 $19.00 + .00

PII: S0020-7683(97)00182-0

CONSTITUTIVE APPROACH TO RATE-INDEPENDENT PROPERTIES OF FILLED ELASTOMERS

M. KALISKE† and H. ROTHERT
Institut für Statik, Universität Hannover, Appelstraße 9a, 30167 Hannover, Germany

(*Received* 3 *September* 1996; *in revised form* 9 *June* 1997)

Abstract—Filled rubber material is used in many technical applications. These structures are often subjected to dynamic loading. Apart from the material's stiffness characteristics dissipative properties are of great importance. At high frequencies rubber material behaves mainly visco-elastically. But at low strain-rate the response is nearly rate-independent. This observation can be interpreted as "internal material friction" and is dealt with in the following article. A constitutive approach is presented, which can be motivated by investigations on the molecular level. This phenomenological description is composed of an elastic model—idealized as an elastic spring—and elasto-plastic Prandtl-elements in parallel. The formulation is derived for small and finite strains. The large strain case is based on a multiplicative decomposition of the deformation gradient. Experimental results and numerical simulations are presented utilizing a mixed finite element formulation to give a robust algorithm and reliable results. © 1998 Elsevier Science Ltd.

1. INTRODUCTION

In the present study we look into a type of rubber material which is employed in a wide range of technical applications. These elastomers are the essential component of e.g. tyres, pneumatic springs or rail brakes. The mentioned class of structures have in common that they are subjected to large deformations as well as to dynamic loading. Therefore, an appropriate constitutive approach has to account for dissipative characteristics and large extensibility of the material.

The principal constituents of the elastomers investigated here are natural and artificial caoutchouc. Long and highly elastic molecules are linked together by the vulcanization process using for example sulfur to form a molecular network. Generally, rubber is modified by filler particles such as carbon-black or silicate to strengthen the mechanical behaviour and to dilute the material in order to reduce costs.

Considering the described class of filled elastomers, a number of typical properties are observed. There is large elastic extensibility with its typical S-shaped load–deflection curve. Moreover, a stiffness reduction is observed during first loading cycles, which converges finally to a stationary situation. This softening, i.e. the so-called Mullins-effect (see Mullins, 1969), results in strain-induced damage mechanisms on the micro-level. Rate-dependent and rate-independent material characteristics are of great importance for stiffness and damping of the oscillations. While several approaches have been proposed to explain most of the mentioned effects, only few publications deal with the rate-independent response. The main concern of this study is the modelling of internal material friction of rubber which can be determined in a quasi-static experiment. Subsequently, the proposed method can easily and consistently be combined with a viscoelastic approach in order to give a realistic material model for a large range of applications.

Recent results concerning time-independent internal material friction of filler modified rubber are given for example by Benner and Platt (1986), Orschall (1990), Lambertz (1993) and Jacob (1995). Generally, these publications have in common that a constitutive empirical function is taken to define the stresses resulting in a static amplitude-dependent hysteresis when a specimen is subjected to cyclic loading. Only a few of the investigations

† Author to whom correspondence should be addressed.

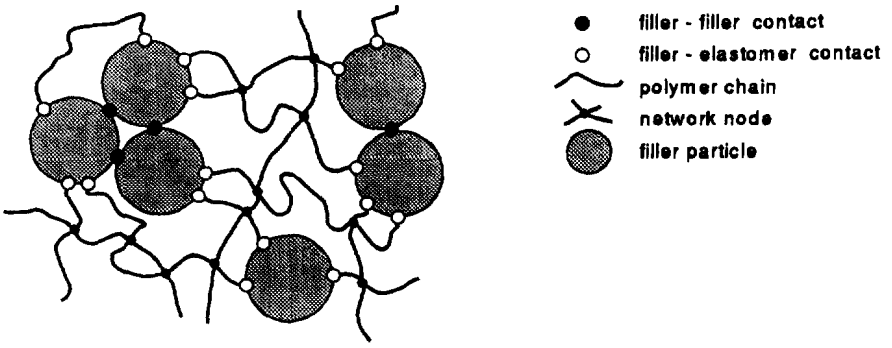

Fig. 1. Micro-structure of a filled polymer network (according to Strauss, 1992).

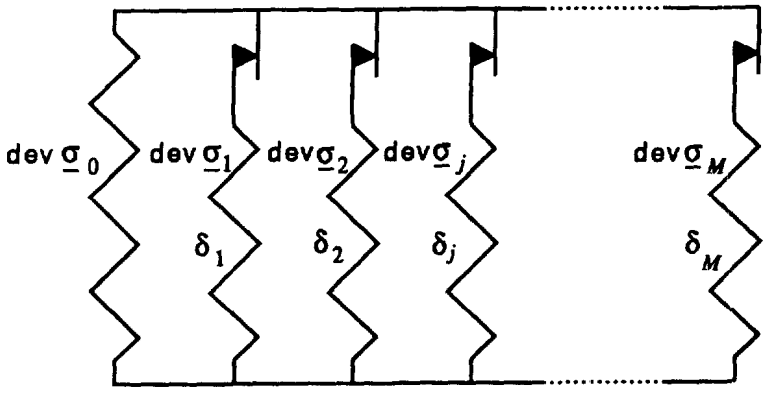

Fig. 2. Generalized Prandtl-model.

(e.g. Orschall, 1990; Jacob, 1995) extend their approach so far that it can be used in a general context like numerical simulations using the finite element method.

Time-independent hysteresis loops obtained when looking into elastomeric material in quasi-static cyclic experiments are reported in the cited literature. All observations agree that even a change in the magnitude of experimental velocity in path-controlled tests does not influence the result significantly. Therefore, it has to be concluded that a viscoelastic model is not adequate to represent the material's response under quasi-static conditions even though both—internal friction and viscoelasticity—contribute to a fast process.

The main idea of the following sections is the introduction of a phenomenological constitutive approach based on linear as well as on finite elastoplasticity suitable for the modelling of internal material friction (Section 3). The proposed generalized Prandtl-element (see Fig. 2) is formulated analogously to the generalized viscoelastic Maxwell-element and, therefore, it is suitable to be used for a consistent coupling of both constitutive contributions. This type of generalized elastoplasticity is motivated in the next section by micromechanical considerations (Section 2). Comments on the determination of the material parameters are given (Section 4). Finally, the model is employed in combination with finite element simulations (Section 5) to illustrate the considerations presented in this paper.

2. MICROMECHANICAL MOTIVATION

The idea of the phenomenological model to characterize rate-independent dissipative behaviour and amplitude-dependent stiffness properties of polymers proposed in this work originates in investigations of Strauss (1992). He explains molecular relations with respect to the mentioned phenomena from the point of view of polymer physics.

Fillers such as carbon-black or silicate are included in polymer networks in order to improve mechanical properties and to reduce material costs. Interactions between filler particles and contacts between network chains and filler particles, which are based on adhesion, are studied by Strauss on the molecular scale. He presents research founding on the molecular slippage model of Dannenberg (1975).

Filler particles are linked together by a large number of polymer chains with different chain lengths (Fig. 1). At a certain state of deformation the critical stretch of a chain λ_{crit} is reached. If the deformation is increased beyond λ_{crit}, the end of this polymer molecule starts an irreversible slipping process on the filler surface. Due to the fact that polymer molecules have different chain lengths, the onset of sliding is found at different macroscopic states of deformation. Additionally, filler particles are deformed plastically when the elastic limit is exceeded and the filler–filler contact is also subjected to plastic slipping.

Strauss describes the different types of forces acting between the particles and derives quantitative expressions characterizing the plastic deformation process. These considerations are confirmed by experiments. Since his costly physical model is established on the micro-scale it is not suitable for numerical simulations of entire structures. But the results of Strauss motivate the introduction of the generalized Prandtl-model (Fig. 2) and its application to rubber material.

The constitutive approach derived here is represented symbolically by arranging a finite number of elastoplastic Prandtl-elements in parallel with an elastic spring. The frictional material elements have ideal-plastic characteristics. Choosing different yield limits results in a formulation which is capable of simulating the described plastic slip process at different macroscopic strain levels as well as the plastic deformation of the filler particles.

Consider an uniaxial extension test, on the molecular level the number of plastic slipping processes is a function of the macroscopic state of deformation. The plastic part of the response is increasing with an increasing deformation. Generally, this relation is nonlinear. The mentioned characteristics are found for the generalized Prandtl-element using ideal plasticity. Here, stiffness is reduced in a nonlinear way depending on the deformation and the response is elastic again for unloading conditions.

3. CONSTITUTIVE MODEL

Analogously to the generalized Maxwell-model a finite number of Prandtl-elements, each consisting of an elastic spring and a rigid-plastic slider, are arranged in parallel (Fig. 2). This way the generalized formulation has an additive structure for small and even for large strains. Different elastoplastic parameters are associated with these symbolic elements. The underlying basic elastic stiffness is represented by the separate spring. The discrete formulation of these symbolic elements results in a material approach which comprises rate-independent and amplitude-dependent stiffness and damping properties.

The basic ideas go back to Masing (1926/1927) who modelled amplitude-depending damping phenomena in the 1920s. Later, Iwan (1967) pursued related methods by arranging elastoplastic elements in parallel and in series for the small strain case. In recent publications of Stein *et al.* (1992, 1993) a discrete overlay-model similar to the proposed type is used in combination with shake-down simulations in a geometrically linear context.

Since a reduction of stiffness is found after the beginning of plastic slipping it seems to be natural to reduce the proposed multi-element approach to a one material element formulation with sophisticated strain hardening characteristics. Due to the fact that a stationary and rate-independent hysteresis is reported for a quasi-static cyclic experiment (see Fig. 9(b)), isotropic hardening is not suitable to take the reduced stationary stiffness beyond plastic yielding into account. Stein *et al.* (1992), (1993) pointed out that an equivalence of a nonlinear kinematic hardening approach with the proposed overlaying of a discrete number of ideal-plastic elements can be shown. In their publications the transition is given for the geometrically linear formulation. Consequently, it could be suggested to reduce the superposition of M elements to one complex material element with hardening behaviour, but deficiencies are encountered for the single-element case. An extension of the shown class of finite elastoplasticity to nonlinear kinematic hardening has not yet been

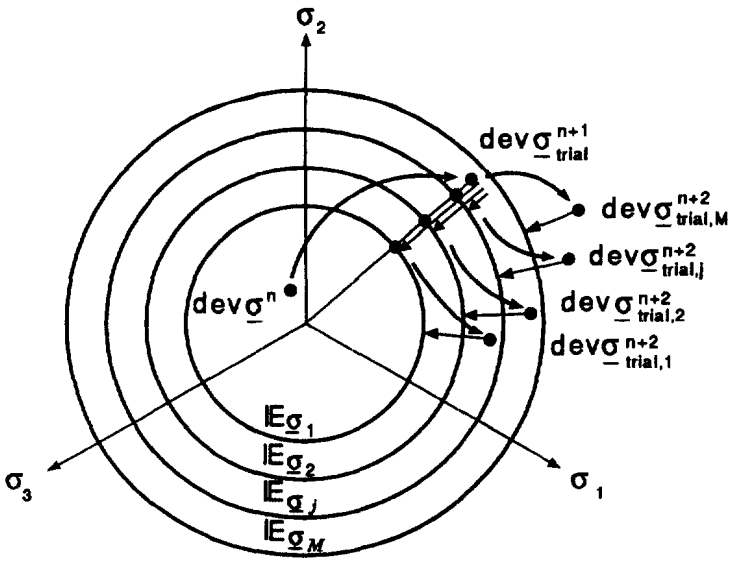

Fig. 3. Generalized Prandtl-model in the principal stress space.

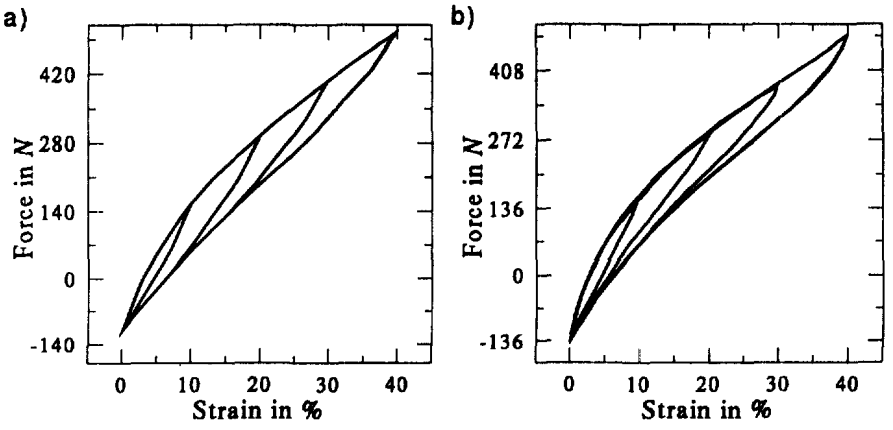

Fig. 4. Cyclic extension test ((a) analytical result, (b) experiment).

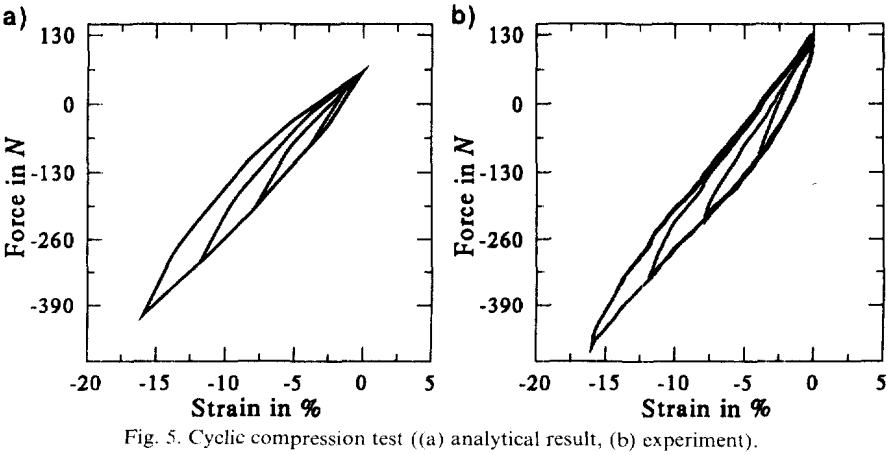

Fig. 5. Cyclic compression test ((a) analytical result, (b) experiment).

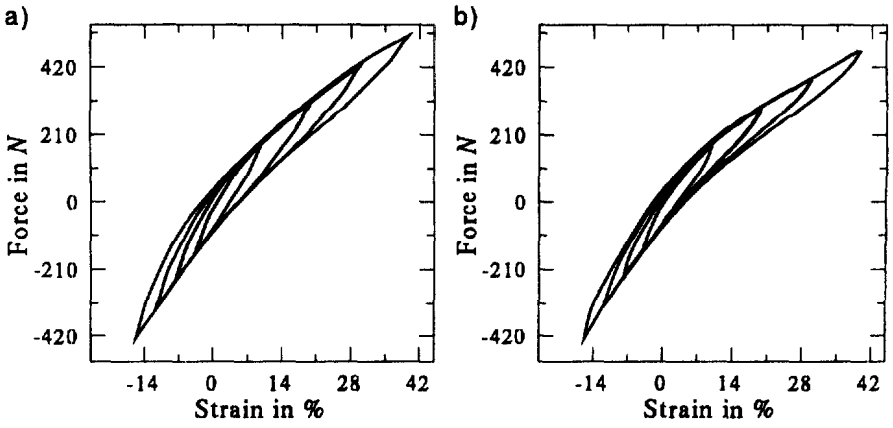

Fig. 6. Cyclic extension-compression test ((a) analytical result, (b) experiment).

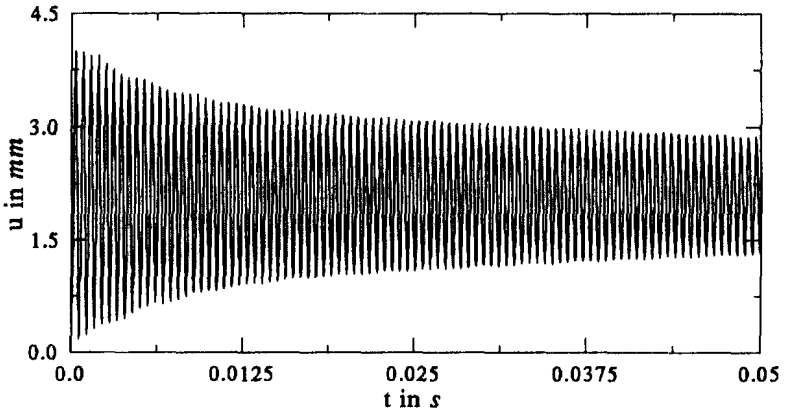

Fig. 7. Free-vibration test.

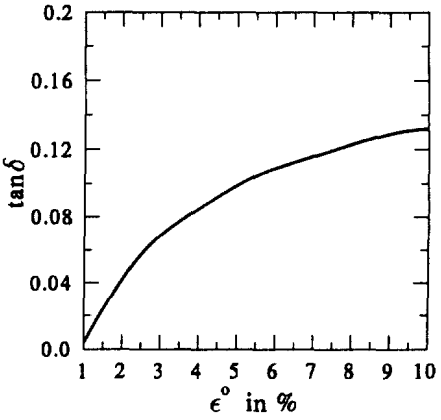

Fig. 8. Amplitude-dependent damping.

published in detail as far as the authors are aware. A certain amount of theoretical work would be necessary to derive the extended approach in order to obtain similar results computed by the superposition model which is already available. Nevertheless, a number of material parameters are required in both cases to formulate a nonlinear hardening function. While the numerical characteristics of the one element to be derived are not known yet, numerical experiments proved stability and quadratic convergence rate of the formulation employed in this paper.

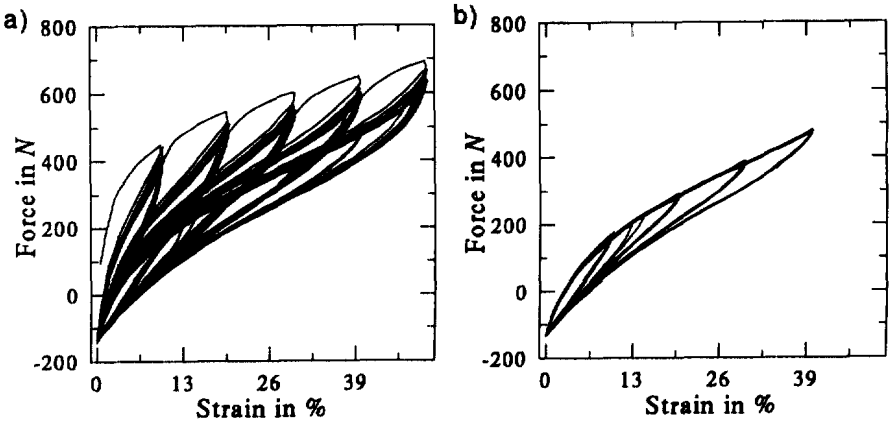

Fig. 9. Cyclic extension test, v = 1 mm/min ((a) 1–9 interval, (b) 6–9 interval).

The reason for energy losses in elastomeric material is twofold. One origin is the viscoelastic frequency-dependent behaviour which is well known and usually introduced by a generalized Maxwell-element. The second contribution, recently recognized and addressed in this paper, comes from the filler–rubber network interaction. Subjecting a rubber sample to a time-dependent deformation the response is surely influenced by both phenomena. In order to take rate-dependent and rate-independent effects simultaneously into account the proposed model is easily extended by Maxwell-elements in parallel. For a slow, i.e. quasi-static deformation, the viscoelastic behaviour is not of great importance and the observed material response exhibits elastoplastic features.

3.1. *Linear elastoplasticity*

In the following section, fundamentals of isothermal linear elastoplasticity are briefly summarized. A detailed description can be found e.g. in Simo and Taylor (1985) and Simo and Hughes (1988). The geometrically linear formulation is meant as a motivation and an illustration of principle structures for the extension to finite strains.

Since an elastic spring and a plastic slider are arranged in series to yield a simple elastoplastic Prandtl-element, total infinitesimal strains are composed additively

$$\boldsymbol{\varepsilon} = \boldsymbol{\varepsilon}^e + \boldsymbol{\varepsilon}^p \tag{1}$$

of elastic $\boldsymbol{\varepsilon}^e$ and irreversible plastic contributions $\boldsymbol{\varepsilon}^p$. Different behaviour with respect to a volumetric or an isochoric deformation is observed in a lot of materials. Therefore, an additive split of the strain tensor

$$\boldsymbol{\varepsilon} = \tfrac{1}{3} I_\varepsilon \mathbf{1} + \operatorname{dev} \boldsymbol{\varepsilon} \tag{2}$$

is accomplished and the inelastic deformation is related only to the volume-preserving part of the deformation $\operatorname{dev} \boldsymbol{\varepsilon}$. The volumetric deformation is based on the first invariant I_ε of the strain tensor $\boldsymbol{\varepsilon}$.

The strain energy function Ψ and the yield function Φ in combination with the principle of positive dissipation for the isothermal case

$$\mathscr{D}^p := \boldsymbol{\sigma} : \dot{\boldsymbol{\varepsilon}} - \dot{\Psi} \geq 0 \tag{3}$$

and the principle of maximum dissipation form the constitutive basis of the plasticity model. The elastic region

$$\mathbb{E}\boldsymbol{\sigma} := \{\boldsymbol{\sigma} \in \mathbb{R}^6 | \hat{\Phi}(\boldsymbol{\sigma}) \leqslant 0\} \tag{4}$$

is defined in the stress space. Based on these fundamentals a standard formulation of plasticity is developed. In the following approach an associated flow rule

$$\dot{\boldsymbol{\varepsilon}}^p = \lambda \frac{\partial \Phi}{\partial \boldsymbol{\sigma}} \tag{5}$$

is used in combination with a yield criterion

$$\hat{\Phi}(\boldsymbol{\sigma}) = \hat{F}(\boldsymbol{\sigma}) - \sqrt{\tfrac{2}{3}}\sigma_y \leqslant 0 \tag{6}$$

for ideal plasticity. The parameter σ_y stands for the yield limit. The function $\hat{F}(\boldsymbol{\sigma})$ is readily computed in case of von Mises plasticity $\hat{F}(\boldsymbol{\sigma}) = \|\operatorname{dev}\boldsymbol{\sigma}\|$ which is employed here. The conditions of loading–unloading

$$\hat{\Phi}(\boldsymbol{\sigma}) \leqslant 0, \quad \lambda \geqslant 0, \quad \lambda\hat{\Phi}(\boldsymbol{\sigma}) = 0 \tag{7}$$

are obtained as a result of the application of the principle of maximum dissipation. The gradient

$$\mathbf{n} = \frac{\partial \Phi}{\partial \boldsymbol{\sigma}} = \frac{\partial F}{\partial \boldsymbol{\sigma}} \tag{8}$$

is a tensor normal to the yield surface in the stress space.

The numerical implementation of the model is founded on the projection algorithm proposed by Wilkins (1964). The integration of the constitutive model yields a stable implicit backward Euler algorithm. Starting from time t_n when the whole situation of the material is known, i.e. total strain $\boldsymbol{\varepsilon}^n$ and plastic strain $\boldsymbol{\varepsilon}^{p,n}$. We are addressing the present time interval $[t_n, t_{n+1}]$. The algorithm splits the solution procedure up in an elastic and a plastic subproblem. The elastic predictor

$$\operatorname{dev}\boldsymbol{\sigma}_{\text{trial}}^{n+1} = 2\mu \operatorname{dev}\boldsymbol{\varepsilon}_{\text{trial}}^{e,n+1} \quad \text{where} \quad \operatorname{dev}\boldsymbol{\varepsilon}_{\text{trial}}^{e,n+1} = \operatorname{dev}(\boldsymbol{\varepsilon}^{n+1} - \boldsymbol{\varepsilon}^{p,n}) \tag{9}$$

and μ is the shear modulus, has to be checked for yielding by evaluating the yield condition

$$\Phi_{\text{trial}}^{n+1} = \|\operatorname{dev}\boldsymbol{\sigma}_{\text{trial}}^{n+1}\| - \sqrt{\tfrac{2}{3}}\sigma_y > 0 \tag{10}$$

in the simple form of ideal von Mises plasticity. The scaling factor β^{n+1} is readily computed from

$$\Phi^{n+1} = \beta^{n+1}\|\operatorname{dev}\boldsymbol{\sigma}_{\text{trial}}^{n+1}\| - \sqrt{\tfrac{2}{3}}\sigma_y = 0 \tag{11}$$

which gives the plastic radial-return correction

$$\operatorname{dev}\boldsymbol{\sigma}^{n+1} = \beta^{n+1}\operatorname{dev}\boldsymbol{\sigma}_{\text{trial}}^{n+1} \tag{12}$$

of the stress predictor back to the yield surface if yielding occurs, i.e. $\Phi_{\text{trial}}^{n+1} > 0$. Similarly, we get the deviatoric elastic strain tensor

$$\operatorname{dev}\boldsymbol{\varepsilon}^{e,n+1} = \operatorname{dev}\boldsymbol{\varepsilon}^{e,n+1}_{\text{trial}} - \Delta\lambda^{n+1}\frac{\operatorname{dev}\boldsymbol{\sigma}^{n+1}_{\text{trial}}}{\|\operatorname{dev}\boldsymbol{\sigma}^{n+1}_{\text{trial}}\|} \tag{13}$$

where

$$\Delta\lambda^{n-1} = \frac{\Phi^{n+1}_{\text{trial}}}{2\mu}. \tag{14}$$

The elastic part of the deformation is stored in a data base to provide the material's history for the next time step.

As shown in Fig. 2 we arrange a finite number of elastoplastic Prandtl-elements in parallel analogously to the generalized viscoelastic Maxwell-model. As a result of the rheological model the stresses have an additive structure

$$\boldsymbol{\sigma} = \boldsymbol{\sigma}_{\text{vol}} + \operatorname{dev}\boldsymbol{\sigma}_0 + \sum_{j=1}^{M}\delta_j \operatorname{dev}\boldsymbol{\sigma}_j \tag{15}$$

where δ_j indicates the portion of the separate contributions to the total stiffness. In the space of principal stresses this model is represented by a number of concentric yield surfaces (Fig. 3). For each yield condition $\hat{\Phi}(\boldsymbol{\sigma})_j$ a radial-return projection is accomplished in case of activating all sliders. The Prandtl-elements superimpose material friction with different plastic characteristics $\sigma_{y,j}$ on the elastic response $\operatorname{dev}\boldsymbol{\sigma}_0$. It is an interesting fact that we describe some kind of kinematic hardening with the proposed model. Even when all sliders with ideal-plastic characteristics are activated, a reduced stiffness will remain because of the single elastic spring in parallel to the Prandtl-elements. But in contrast to "real" work hardening the yield stresses $\sigma_{y,j}$ are not modified by the deformation. The resulting hysteresis is stationary in a cyclic test with a constant strain amplitude.

This formulation can be linearized in closed form and yields the tangent operator of the Newton-procedure

$$\begin{aligned}\underline{\underline{\mathbb{C}}}^{ep} &:= \frac{\partial\boldsymbol{\sigma}}{\partial\boldsymbol{\varepsilon}_{\text{trial}}} \\ &= \underline{\underline{\mathbb{C}}}^{e}_{\text{vol}} + \underline{\underline{\mathbb{C}}}^{e}_{\text{iso}} + \sum_{j=1}^{M}\delta_j\left[\beta\underline{\underline{\mathbb{C}}}^{e}_{\text{iso}} - \frac{2\mu\beta}{\|\operatorname{dev}\boldsymbol{\sigma}_{\text{trial}}\|^2}\operatorname{dev}\boldsymbol{\sigma}_{\text{trial}}\otimes\operatorname{dev}\boldsymbol{\sigma}_{\text{trial}}\right]_j\end{aligned} \tag{16}$$

which ensures the quadratic rate of convergence of the iterative process when solving the nonlinear system of equations of the finite element discretization. Simo and Taylor (1985) point out the importance of the consistent linearization of the stress integration algorithm.

3.2. *Finite elastoplasticity*

The constitutive approach introduced in the preceding subsection is extended to finite strains in order to serve as a constitutive model for numerical simulations of rubber structures. The proposed formulation is suitable for moderate elastic and moderate plastic strains, i.e. the strain is restricted to approximately 50%, which is sufficient for a large number of technical applications. Among others Weber and Anand (1990), Eterovic and Bathe (1990) and Simo (1992) recently contributed to the field of multiplicative elastoplasticity. The employed formulation is based on developments of Miehe and Stein (1992).

In contrast to the additive split of the deformation in the linear case (1), the basic kinematic quantity of the geometrically nonlinear regime—the deformation gradient $\mathbf{F}$—is decomposed multiplicatively

$$\mathbf{F} = \mathbf{F}^e\mathbf{F}^p \tag{17}$$

into an elastic $\mathbf{F}^e$ and a plastic portion $\mathbf{F}^p$. Thus, a so-called plastic intermediate configuration is defined which goes back to Lee (1969). The following ideal-plastic and isothermal model is derived with respect to the current configuration, and, as a consequence, is restricted to isotropic material.

The constitutive model shown is of the same structure as the small strain approach. The strain energy function Ψ, the yield function Φ and the evaluation of the two dissipation principles mentioned lead to the final formulation. The principal of positive dissipation

$$\mathscr{D}^p := \boldsymbol{\tau} : \mathbf{l} - \dot{\Psi} \geqslant 0 \tag{18}$$

where $\mathbf{l} := \dot{\mathbf{F}}\mathbf{F}^{-1}$ is the spatial velocity gradient, yields the constitutive hyper-elastic equation for the Kirchhoff stress tensor

$$\boldsymbol{\tau} = 2\frac{\partial \Psi}{\partial \mathbf{b}}\mathbf{b} \tag{19}$$

using the left Cauchy–Green tensor $\mathbf{b}$ and a reduced dissipation inequality. The hyper-surface defined by $\hat{\Phi}(\boldsymbol{\tau})$

$$\mathbb{E}_\tau := \{\boldsymbol{\tau} \in \mathbb{R}^6 | \hat{\Phi}(\boldsymbol{\tau}) \leqslant 0\} \tag{20}$$

separates the elastic and the plastic region in the stress space. Equivalent to eqn (5) the associated flow rule is obtained as

$$-\frac{1}{2}\mathscr{L}_v(\mathbf{b}^e)\mathbf{b}^{e,-1} = \lambda\frac{\partial \Phi}{\partial \boldsymbol{\tau}} \tag{21}$$

using the Lie-derivative $\mathscr{L}_v(\mathbf{b}^e)$ of the left Cauchy–Green tensor $\mathbf{b}^e$. The conditions for loading and unloading

$$\hat{\Phi}(\boldsymbol{\tau}) \leqslant 0, \quad \lambda \geqslant 0, \quad \lambda\hat{\Phi}(\boldsymbol{\tau}) = 0 \tag{22}$$

are determined through the principle of maximum dissipation. From the yield criterion for finite ideal von Mises plasticity

$$\hat{\Phi}(\boldsymbol{\tau}) = \hat{F}(\boldsymbol{\tau}) - \sqrt{\tfrac{2}{3}}\sigma_y \leqslant 0 \tag{23}$$

where $\hat{F}(\boldsymbol{\tau}) = \|\mathrm{dev}\,\boldsymbol{\sigma}\|$. results the tensor

$$\mathbf{n} = \frac{\partial \Phi}{\partial \boldsymbol{\tau}} = \frac{\partial F}{\partial \boldsymbol{\tau}} \tag{24}$$

normal to the hyper-surface $\hat{\Phi}(\boldsymbol{\tau})$ which is the boundary of the elastic region.

As mentioned above, the constitutive basis of the material formulation is the distinction between volumetric and isochoric parts of the deformation which results in a splitted strain energy function

$$\Psi = \hat{U}(J) + \hat{W}(\bar{\mathbf{b}}) \tag{25}$$

where $J = \det \mathbf{F}$ and $\bar{\mathbf{b}} = \bar{\mathbf{F}}\bar{\mathbf{F}}^T$, using the volume-preserving part of the deformation gradient $\bar{\mathbf{F}} = J^{-(1/3)}\mathbf{F}$. This way the kinematic quantity is decomposed multiplicatively

$$\mathbf{F} = (J^{1/3}\mathbf{1})\bar{\mathbf{F}}^e\mathbf{F}^p \tag{26}$$

analogously to the additive split of linear strains [eqn (2)]. It turned out that it is advantageous for the algorithmic formulation of the model to use the logarithmic strain energy function

$$W = \frac{\mu}{4}\ln^2 \bar{\mathbf{b}} \tag{27}$$

where μ is an elastic material parameter. The computation of isotropic tensor-valued tensor functions is based on a spectral decomposition of the quantities (see e.g. Miehe, 1993).

The accompanying elastoplastic algorithm has the same structure as for linear elastoplasticity and, therefore, it is very efficient. The elastic predictor

$$\operatorname{dev}\boldsymbol{\tau}^{n+1}_{\text{trial}} = \mu \ln \bar{\mathbf{b}}^{e,n+1}_{\text{trial}} \tag{28}$$

is computed by using the elastic predictor of the deformation

$$\bar{\mathbf{b}}^{e,n+1}_{\text{trial}} := \bar{\mathbf{F}}^{n+1}(\mathbf{C}^{p,n})^{-1}(\bar{\mathbf{F}}^{n+1})^T. \tag{29}$$

The intermediate plastic configuration of the last converged step is taken into consideration state by $(\mathbf{C}^{n,p})^{-1}$. The elastic trial eqn (28) is followed by a plastic correction according to the standard radial-return method. The von Mises yield criterion for ideal plasticity

$$\Phi^{n+1}_{\text{trial}} := \|\operatorname{dev}\boldsymbol{\tau}^{n+1}_{\text{trial}}\| - \sqrt{\tfrac{2}{3}}\sigma_y \tag{30}$$

is utilized in here and the projection of the Kirchhoff stress tensor to the yield surface

$$\operatorname{dev}\boldsymbol{\tau}^{n+1} = \beta^{n+1}\operatorname{dev}\boldsymbol{\tau}^{n+1}_{\text{trial}} \tag{31}$$

is accomplished analytically in case of $\Phi^{n+1}_{\text{trial}} > 0$ by evaluating β^{n+1} from

$$\Phi^{n+1} = \beta^{n+1}\|\operatorname{dev}\boldsymbol{\tau}^{n+1}_{\text{trial}}\| - \sqrt{\tfrac{2}{3}}\sigma_y = 0. \tag{32}$$

The current plastic intermediate configuration

$$(\mathbf{C}^{p,n+1})^{-1} = (\bar{\mathbf{F}}^{n+1})^{-1}\exp(\beta^{n+1}\ln\bar{\mathbf{b}}^{e,n+1}_{\text{trial}})(\bar{\mathbf{F}}^{n+1})^{-T} \tag{33}$$

forms the basis for the next load step.

Using the multiplicative elastoplastic approach shown above, a generalized Prandtl-element suitable for finite strains is introduced. The model is formulated on the constitutive level and has an additive structure for the Kirchhoff stresses

$$\boldsymbol{\tau} = \boldsymbol{\tau}_{\text{vol}} + \operatorname{dev}\boldsymbol{\tau}_0 + \sum_{j=1}^{M}\delta_j \operatorname{dev}\boldsymbol{\tau}_j \tag{34}$$

analogously to linear strains because of the material elements in parallel. The contribution of each Prandtl-element to the total stiffness is indicated by scalar factors δ_j. The radial-return projection of the stresses $\operatorname{dev}\boldsymbol{\tau}_{\text{trial},j}$ as well as the update of the intermediate configuration $(\mathbf{C}^p)^{-1}_j$ is carried out for each element if plastic yielding occurs. The linearization of the integration procedure is derived analytically to give the algorithmic tangent modulus

$$\underline{\underline{c}} = \underline{\underline{c}}^{e}_{\mathrm{vol}} + \underline{\underline{c}}^{e}_{\mathrm{iso}} + \sum_{j=1}^{M} \delta_j \left[\beta \underline{\underline{c}}^{e}_{\mathrm{iso}} - \frac{2\mu\beta}{\|\mathrm{dev}\,\boldsymbol{\tau}_{\mathrm{trial}}\|^2} \mathrm{dev}\,\boldsymbol{\tau}_{\mathrm{trial}} \otimes \mathrm{dev}\,\boldsymbol{\tau}_{\mathrm{trial}} \right]_j \tag{35}$$

in the current configuration (see also Miehe and Stein, 1992) which can be employed in finite element computations.

4. PARAMETER IDENTIFICATION

The main goal of this article is the introduction of a constitutive strategy to predict the mechanical behaviour of a class of elastomers which have filler improved features. On the one hand details about the rubber blends cannot be published because the recipes of these mixtures are confidential. On the other hand we are looking at mechanical characteristics and their phenomenological modelling. Therefore, the chemical composition of the rubber material investigated is of secondary importance.

The constitutive approach is a combination of discrete material elements. The contribution of each element δ_j to the total stiffness has to be determined. Apart from this scalar quantity further material parameters are introduced by the two basic constitutive functions. The strain energy function Ψ and the yield function Φ define the elastic and the plastic model used. In principle, any elastic approach is suitable. Nevertheless, the simple logarithmic potential function (27) with the elastic quantity μ is sufficient for a large number of cases. The ideal-plastic von Mises yield function Φ comprises the yield limit σ_y which stands for the activation of the ideal-plastic sliders. In summary, one elastic modulus μ and pairs of $(\delta_j, \sigma_{y,j})$ for each Prandtl-element j have to be determined. The physical behaviour of polymer chains is not directly formulated by the presented model because of its phenomenological character. Thus, a physical interpretation of the material parameters is not meaningful.

The number of elements and material parameters, respectively, required for a realistic simulation, depends on the strain range and the shape of the hysteresis to be represented. This corresponds to the generalized viscoelastic Maxwell-element which has to be composed of a particular number of elements in order to reproduce a certain frequency range.

We use a set of uniaxial extension, compression and combined extension-compression tests as starting point for the parameter identification process. The stationary part of these quasi-static cyclic experiments is considered. The advantage of the mentioned type of investigations is the fact that they can be described by an analytical formulation of the material model when incompressibility is assumed ($J = \det \mathbf{F} \equiv 1$). Therefore, stochastic methods like evolution strategies are advantageous algorithms for the parameter identification. Core of this approach is the formulation of an optimization problem which is iteratively solved using genetic algorithms. It minimizes the error between experimental data and analytical expression.

The result of an identification procedure is given by Table 1 and Figs 4–6. The set of parameters (Table 1) computed iteratively via a simple evolution process is valid for the three different experiments depicted by Figs 4(b)–6(b). These cyclic tests were taken into consideration for the parameter determination and they are compared with the analytical results (Figs 4(a)–6(a)) utilizing these material data. An improved agreement between tests and analytical simulation can be expected when the identification algorithm is developed further. Taking more experiments into account, e.g. shear tests, is feasible and enlarges the validity range of the parameters.

Table 1. Material data (modulus $\mu = 1.500$ N/mm^2)

j	1	2	3	4	5	6	7
δ_j [-]	2.816^{-1}	1.800^{-1}	1.150^{-9}	7.100^{-1}	3.616^{-1}	2.107^{-1}	5.773^{-2}
$\sigma_{y,j}$ [N/mm^2]	6.847^{-2}	1.004	1.975^{-8}	5.668^{-2}	1.934^{-1}	2.731^{-1}	1.513

5. NUMERICAL EXAMPLES

Numerical simulations presented below illustrate the principal characteristics of the model. Furthermore, a comparison with experimental work points out the capabilities of the formulation.

Example 5.1.

A certain material behaviour is approximated by a generalized Prandtl-element consisting of six elastoplastic elements for the small strain case. A cantilever beam is investigated in a free-vibration test (Fig. 7). The diagram showing the tip-deflection curve as a function of time exhibits large damping at the beginning. The dissipation is reduced during the course of vibration. Amplitude-dependence of the material can already be seen from this result.

When the loss factor $\eta = \tan\delta$ is evaluated as a function of the strain, amplitude-dependency of damping becomes apparent. The angle δ indicates the phase-shift between a harmonic stress-function and the accompanying strain-function which is found because of inelastic material characteristics. Therefore, it is a quantitative measure for dissipation. The shift-factor can be determined by employing Fourier's analysis to the time-dependent stress- and strain-function of a selected point in a path-controlled simulation. Figure 8 clearly depicts the nonlinear relation between damping and strain amplitude observed already in Fig. 7. Here, a harmonic path controlled deformation at different amplitudes ε^0 is investigated. From the diagram the increase of dissipation due to a rise of the amplitude ε^0 is seen.

Example 5.2.

A cylindrical rubber-specimen (length = 50 mm, diameter = 20 mm) is investigated in cyclic extension and compression tests. A path-controlled deformation is applied at the velocity of $v = 1$ mm/min and $v = 50$ mm/min. The underlying constitutive model used in the numerical simulation of this experiment is composed of seven Prandtl-elements and an elastic spring in parallel.

Half of the specimen is discretized by 60 Q2/P1-elements (according to Simo and Taylor, 1991), making partial use of the symmetries. These mixed elements account for almost complete incompressibility of rubber material. Figure 10 depicts the finite element simulation at maximum extension (+50%), maximum compression (−20%) and the undeformed reference state.

For the experimental investigation, the cylindrical rubber specimen was subjected to nine load intervals at different strain amplitudes (Fig. 9). Loading and unloading went through each interval ten times. The deformation was increased in steps of 10% up to the maximum of 50% extension at the fifth interval, and then it was reduced again. The graph of the whole experimental load displacement history does not give a clear impression (1–9

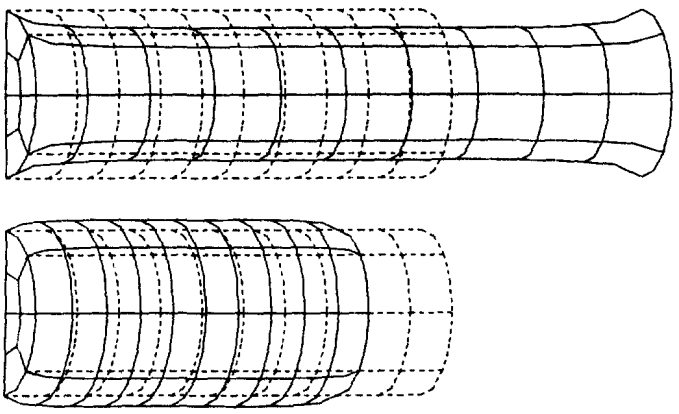

Fig. 10. Deformed configurations.

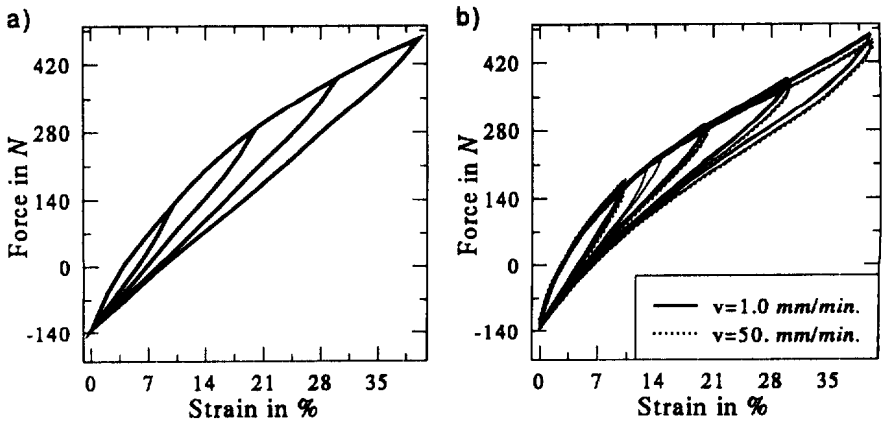

Fig. 11. Cyclic extension test ((a) FE-computation, (b) experiment).

interval). But looking at the intervals when reducing the load amplitudes, all ten cycles for a particular strain amplitude coincide (6–9 interval). In the second part of the experiment, damage phenomena like the Mullins-effect are reduced and we can take this part of the investigation for a comparison. The compression test was carried out equivalently. The specimen was subjected to the total deformation in steps of -4% up to the maximum compression -20% in the fifth interval. Then the compression was reduced again. Parameter identification, described in Section 4, is based on this type of experiments.

Both experiments are simulated numerically by finite element computations (Fig. 10). Numerical and experimental results are compared (Figs 11 and 12) for the stationary part of the test (6–9 interval). The plots depict the uniaxial force as a function of the strain. The experimental hysteresis loops are quantitatively well approximated by the computations. Even the shape of the hysteresis is reproduced in principal. The reason for the slight discrepancies of numerical result and experiment is the simple logarithmic strain energy function. If more elaborate elastic models are employed, e.g. Ogden's (1982) approach, improved results with respect to the shape of the hysteresis can be expected.

For the computations shown the modulus of the purely elastic spring was set to $\mu = 1.336\ \mathrm{N/mm^2}$. We identified the elastoplastic material parameters only on the basis of the extension test (see Table 2). Afterwards, we carried out the compression test and found out that the chosen set of material data is also appropriate for this loading. Comparing the finite element and the experimental results we can conclude that the hypothesis of rate-independent inelastic behaviour for filled rubber material is confirmed. The influence of the strain-rate is not significant in the present case and we can model this phenomenon by a

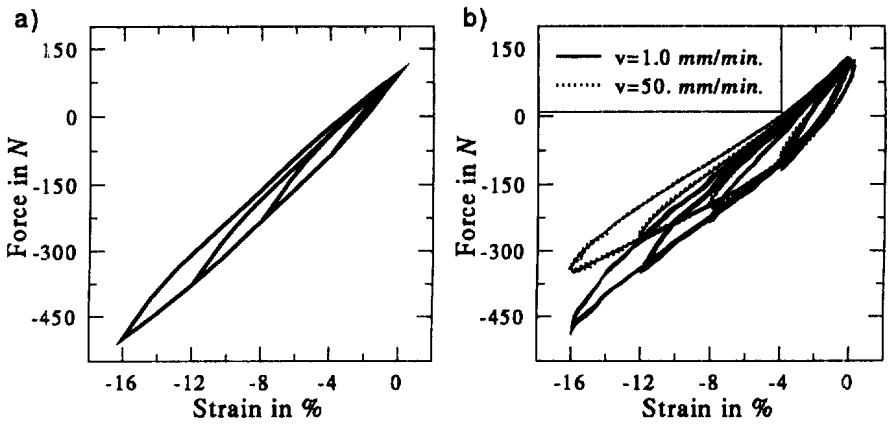

Fig. 12. Cyclic compression test ((a) FE-computation, (b) experiment).

Table 2. Material data (modulus $\mu = 3.34$ N/mm^2, Poisson's ratio $\nu = 0.497$)

j	1	2	3	4	5	6	7
σ_j [-]	0.04	0.06	0.06	0.08	0.10	0.20	0.30
$\sigma_{y,j}$ [N/mm^2]	2.0	1.5	1.0	0.8	0.6	0.2	0.1

generalized elasto-plastic formulation quite well. The static hysteresis of rubber material is simulated realistically at finite strains by the generalized Prandtl-element.

6. CONCLUSIONS

Rate-independent material properties of filled rubber, which are interpreted as plastic slip on the micromechanical level, were experimentally observed. In order to simulate the behaviour of elastomeric structures realistically, an elastoplastic generalized model suitable for small and finite strains was proposed. Finite element computations prove that the model is suitable for use in large scale static and dynamic simulations. Good agreement was obtained for the static hysteresis and even for a quantitative comparison. The results shown look promising. An extension to improved elastic formulations combined with plasticity would round off the mechanical model, but results should not in principal differ from the shown data. Consequently, the proposed model may serve as a component of a complex material formulation which also incorporates viscoelastic properties to yield a realistic approach to filled rubberlike material.

Acknowledgement—The authors gratefully acknowledge the support of the Continental AG in providing experimental data and financial assistance.

REFERENCES

Benner, J. and Platt, W. (1986) Kupplungsausfallkriterien. Forschungsvereinigung Antriebstechnik e.V., Heft 221, Frankfurt.

Dannenburg, E. M. (1975) The effects of surface chemical interactions on the properties of filler-reinforced rubbers. *Rubber Chemistry and Technology* **48,** 410–444.

Eterovic, A. L. and Bathe, K.-J. (1990) A hyperelastic-based large strain elastoplastic constitutive formulation with combined isotropic-kinematic hardening using the logarithmic stress and strain measures. *International Journal of Numerical Methods in Engineering* **30,** 1099–1114.

Iwan, W. D. (1967) On a class of models for the yielding behavior of continuous and composite systems. *ASME, Journal of Applied Mechanics* **34,** 612–617.

Jacob, H.-G. (1995) Zur Berechnung lokaler Deformationen in Luftfederbalgwänden. Dissertation, Universität Hannover.

Lambertz, S. (1993) Nichtlineares Materialgesetz für technische Gummiwerkstoffe mit deformationsabhängigen Eigenschaften und seine experimentelle Überprüfung an Gummifederelementen. Dissertation, Rheinisch-Westfälische Technische Hochschule Aachen.

Lee, E. H. (1969) Elastic–plastic deformation at finite strains. *ASME, Journal for Applied Mechanics* **36,** 1–6.

Masing, G. (1926/1927) Berechnung von Dehnungs- und Stauchungslinien auf Grund von inneren Spannungen. *Wissenschaftliche Veröffentlichungen aus dem Siemens-Konzern* **5,** 135–141.

Masing, G. and Mauksch, W. (1926/1927) Über das Verhalten von kalt gerecktem Messing bei Zug- und Stauchbelastung. *Wissenschaftliche Veröffentlichungen aus dem Siemens-Konzern* **5,** 142–155.

Miehe, C. and Stein, E. (1992) A canonical model of multiplicative elasto-plasticity. Formulation and aspects of the numerical implementation. *European Journal of Mechanics, A/Solids* **11,** 25–43.

Miehe, C. (1993) Computation of isotropic tensor functions. *Communications in Numerical Methods in Engineering* **9,** 889–896.

Mullins, L. (1969) Softening of rubber by deformation. *Rubber Chemistry and Technology* **42,** 339–362.

Ogden, R. W. (1982) Elastic deformations of rubberlike solids. *Mechanics of Solids.* The Rodney Hill 60th Anniversary Volume, ed. H. G. Hopkins, M. J. Sewell. Pergamon Press, Oxford.

Orschall, B. (1990) Mathematisches Modell für die Simulation viskoelastischer and reinbungsbehafteter Elastomereigenschaften. Dissertation, Rheinisch-Westfälische Technische Hochschule Aachen.

Simo, J. C. and Taylor, R. L. (1985) Consistent tangent operators for rate-independent elastoplasticity. *Computer Methods in Applied Mechanics and Engineering* **48,** 101–118.

Simo, J. C. and Hughes, T. J. R. (1988) Elastoplasticity and viscoplasticity. Preprint, Springer Verlag, New York.

Simo, J. C. and Taylor, R. L. (1991) Quasi-incompressible finite elasticity in principal stretches. Continuum basis and numerical algorithms. *Computer Methods in Applied Mechanics and Engineering* **85,** 273–310.

Simo, J. C. (1992) Algorithms for static and dynamic multiplicative plasticity that preserve the classical return mapping schemes of the infinitesimal theory. *Computer Methods in Applied Mechanics and Engineering* **99,** 61–112.

Stein, E., Zhang, G. and König, J. A. (1992) Shakedown with nonlinear strain-hardening including structural computation using finite element method. *International Journal of Plasticity* **8,** 1–31.

Stein, E., Zhang, G. and Huang, Y. (1993) Modeling and computation of shakedown problems for nonlinear hardening materials. *Computer Methods in Applied Mechanics and Engineering* **103,** 247–272.

Strauss, M. (1992) Struktur gefüllter Vulkanisate und Mechanismen der Verstärkung. Dissertation, Universität Ulm.

Weber, G. and Anand, L. (1990) Finite deformation constitutive equations and a time integration procedure for isotropic, hyperelastic–viscoplastic solids. *Computer Methods in Applied Mechanics and Engineering* **79,** 173–202.

Wilkins, M. L. (1964) Calculation of elastic–plastic flow. *Methods of Computational Physics* **3,** 211–263.